Amoeba Predation of *Cryptococcus*: A Quantitative and Population Genomic Evaluation of the Accidental Pathogen Hypothesis

Thomas J. C. Sauters, Cullen Roth, Debra Murray, Sheng Sun, Anna Floyd-Averette, Chinaemerem U. Onyishi, Robin C. May, Joseph Heitman, Paul Magwene

Abstract

The “Amoeboid Predator-Fungal Animal Virulence Hypothesis” posits that interactions with environmental phagocytes shape the evolution of virulence traits in fungal pathogens. In this hypothesis, selection to avoid predation by amoeba inadvertently selects for traits that contribute to fungal escape from phagocytic immune cells. Here, we investigate this hypothesis in the human fungal pathogens *Cryptococcus neoformans* and *Cryptococcus deneoformans*. Applying quantitative trait locus (QTL) mapping and comparative genomics, we discovered a cross-species QTL region that is responsible for variation in resistance to amoeba predation. In *C. neoformans*, this same QTL was found to have pleiotropic effects on melanization, an established virulence factor. Through fine mapping and population genomic comparisons, we identified the gene encoding the transcription factor *BZP4* that underlies this pleiotropic QTL and we show that decreased expression of this gene reduces melanization and increases susceptibility to amoeba predation. Despite the joint effects of *BZP4* on amoeba resistance and melanin production, we find no relationship between *BZP4* genotype and escape from macrophages or virulence in murine models of disease. Our findings provide new perspectives on how microbial ecology shapes the genetic architecture of fungal virulence, and suggests the need for more nuanced models for the evolution of pathogenesis that account for the complexities of both microbe-microbe and microbe-host interactions.

Introduction

For many free-living pathogens, there is no host-to-host transmission and infection of a host is not an obligatory stage of their life cycle. Pathogenesis in these cases is considered opportunistic, and key traits that facilitate virulence are not likely to have evolved due to adaptation to the host directly [1, 2]. Rather, the ability to cause disease is hypothesized to be an unintentional byproduct of evolving in a varied, stressful environment ("accidental virulence"; [3]). This raises the question: "What environmental interactions contribute to the evolution of virulence?"

A prominent hypothesis proposed for many environmental pathogens suggests that predator-prey interactions between microbes drive the evolution of traits advantageous to pathogenesis [4]. Chief among the predators that have been suggested as relevant to the evolution of virulence traits are amoebae. For example, bacterial pathogens such as *Bordetella*, *Legionella*, and *Pseudomonas*, as well as the fungal pathogens *Paracoccidioides*, *Cryptococcus*, and *Aspergillus*, are all preyed upon by phagocytic amoebae [5, 6, 7, 8, 9, 10, 11]. Amoebae share many similarities with macrophages and other primary immune cells that microbial pathogens encounter during infection of mammalian hosts. These similarities include immune receptors tht detect microbila PAMPs, actin mediated phagocytosis, acidification, nitrosative stress, and metalo-ion toxicity in the phagosome. [12, 13, 14, 15]. In light of this, it has been proposed that amoebae may serve as "training grounds" for intracellular pathogens [16]. For fungi in particular, the idea that interactions with amoebae in the environment drives the selection of fungal traits necessary for survival during mammalian infection has been termed the "Amoeboid Predator-Fungal Animal Virulence Hypothesis" [17].

For the fungal pathogen *Cryptococcus neoformans*, interactions with free-living amoebae have been documented for nearly 100 years [18]. Amoebae are found in many of the same niches that *C. neoformans* inhabits, and *C. neoformans* is actively consumed by amoebae isolated from pigeon guano [19]. *C. neoformans*, and the amoebae that consume it, are globally distributed [20, 21]. *C. neoformans* is a saprophytic fungus; however, it has the ability to cause disease in vulnerable human populations, primarily infecting individuals with reduced immunity due to factors such as HIV/AIDS or immunosuppressive drug treatments [22, 23, 24, 25]. *C. neoformans* infections in mammals are facilitated by a variety of traits including: a polysaccharide capsule [26, 27, 28], the ability to grow at high temperatures [29, 30], the production of melanin [31, 32], and a battery of secreted phospholipases [33, 34] and ureases [35, 36]. These same virulence factors act as defense mechanisms against amoebae [37, 38, 28]. Passaging *C. neoformans* strains with amoebae increases virulence factor presentation and results in enhanced pathogenicity in mammalian tissue culture, insects, and mouse models of infection [39, 40]. These findings support the hypothesis that amoebae may play a key role in the evolution of *C. neoformans* virulence factors. However, most studies that characterize the similarities between *Cryptococcus*'s interactions with amoebae and with animal immune systems have targeted known virulence genes, primarily through gene deletion studies. Furthermore, these studies analyzed a small number of *Cryptococcus* strain

backgrounds. Focusing on previously identified genes, in a limited number of strains, may bias or obscure other genes and pathways important for amoeba resistance.

In this study we ask, "Do alleles important for fungal survival with amoeba correspond to known virulence genes?" To answer this question, we employed quantitative trait locus (QTL) mapping to identify genomic regions and allelic variants that contribute to resistance against amoeba predation in two pathogenic species of *Cryptococcus*, *C. neoformans* and *C. deneoformans*. For both species we identified major effect QTL. Surprisingly, these QTL regions were found to be homologous between the species. For *C. neoformans*, the amoeba resistance QTL identified is also a melanization QTL. By combining of comparative genomics and genetic engineering we identified a likely causal variant for this QTL region, a 1.8 kb deletion upstream of the transcription factor encoding gene *BZP4*. Disruption of this region leads to altered transcription of *BZP4* and other genes, and these transcriptional differences are in turn associated with reduced amoeba resistance and melanization capacity. Despite alterations in amoeba resistance and melanization associated with disregulation of *BZP4*, comparative analysis suggests that *BZP4* is not required for virulence in mice or macrophages. In addition, no relationship is found between genetic variation in the ability to resist amoeba predation and virulence in mouse models of infection. Our findings both advance the understanding of the genetic architecture of virulence traits, but also suggest the need for a more nuanced perspective on the evolutionary and ecological interactions that have shaped microbial pathogenesis.

Results

Comparison of Amoeba Resistance in Diverse *C. neoformans* Strains

We developed a plate-based assay to quantify *Cryptococcus* resistance to predation by the amoeba, *Acanthamoeba castellanii* (Fig. 1A; [41]). Briefly, an established lawn of *Cryptococcus* cells was inoculated with a drop of amoeba. After a defined period of time, the cleared (consumed) portion of the lawn is quantified and used as a measure of resistance. The larger the clearance area, the less resistant the cells are to amoeba consumption.

This amoeba resistance assay was applied to a diverse set of *C. neoformans* strains that represent major sub-lineages within this species (Table 1). This assay revealed extensive variation in amoeba resistance between strain backgrounds (Fig. 1C). Notably, there is no simple relationship between the site of collection and amoeba resistance; clinical strains isolated from patient samples exhibited both resistant and sensitive amoeba resistance phenotypes.

Mapping Populations and Genome Sequencing

From our collection of genetically diverse strains, strains of opposite mating type (*MAT***a**-*MAT*α) were identified that differed in their resistance to amoeba. We carried out pairwise mating tests to identify strain pairs with sporulation and germination efficiency suitable for establishing a large

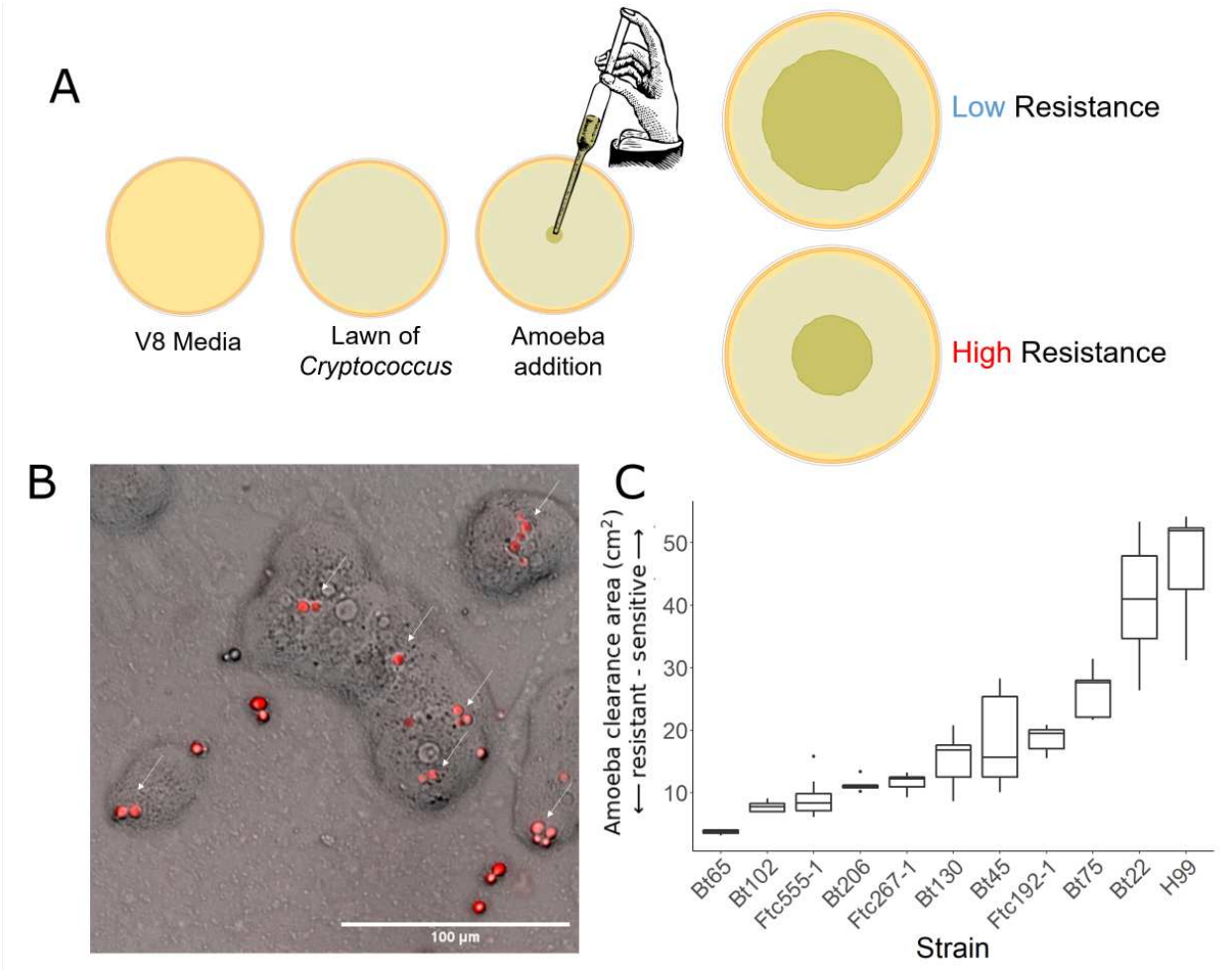

Figure 1: **Amoeba resistance varies between strains of *C. neoformans*. A.** A schematic overview of the amoeba resistance assay. A lawn of *Cryptococcus* is grown on V8 media for 60 hours. *A. castellanii* are added to the center of the lawn. *A. castellanii* consume the cells across the plate for a period of 12 or 18 days (based on amoeba activity). *Cryptococcus* strains able to resist amoeba have smaller areas of consumption when imaged. **B.** *A. castellanii* in co-culture with *C. neoformans* expressing RFP on solid V8 media. White arrows indicate examples of *C. neoformans*- amoeba interaction. **C.** Boxplots representing amoeba resistance phenotypes for a diverse set of *C. neoformans* strains after 18 days of amoeba co-culture. The x-axis displays the strains assayed. The y-axis represents the area the amoeba consumed. Smaller clearance areas indicate greater resistance to amoeba.

Table 1: Genetically diverse *C. neoformans* strains surveyed for amoeba resistance.

Strain	Lineage	Site	Source
Bt102	VNBI	clinical	Litvintseva et al. (2003)
Bt22	VNBI	clinical	Litvintseva et al. (2003)
Bt45	VNBI	clinical	Litvintseva et al. (2003)
Ftc192-1	VNBI	environmental	Chen et al. (2015)
Ftc267-1	VNBI	environmental	Chen et al. (2015)
FTC555-1	VNBI	environmental	Chen et al. (2015)
Bt1	VNBII	clinical	Litvintseva et al. (2003)
Bt103	VNBII	clinical	Litvintseva et al. (2003)
Bt206	VNBII	clinical	Litvintseva et al. (2003)
Bt65	VNBII	clinical	Litvintseva et al. (2003)
Bt75	VNBII	clinical	Litvintseva et al. (2003)
AD1-7a	VNI	clinical	Dromer et al. (2007)
Bt130	VNI	clinical	Litvintseva et al. (2003)
H99	VNI	clinical	Perfect et al. (1980)
KN99a	VNI	laboratory	Nielsen et al. (2003)

genetic mapping population. *C. neoformans* strains Bt22 and Ftc555-1 were chosen for further analysis based on spore viability and differences in their amoeba resistance. The low-resistance strain Bt22 (*MAT***a**) is a clinical isolate while the high-resistance strain Ftc555-1 (*MAT*α) is an environmental isolate collected from a mopane tree; both strains were collected in Botswana [46]. By manual spore dissection, we isolated 384 progeny from a cross between these two strains. The genomes of these progeny were then sequenced on the Illumina NovaSeq 6000 platform to an average depth of ~15$\times$. Based on the resulting sequence data, the progeny were filtered based on criteria including sequencing depth, read quality, elevated ploidy, and clonality. After filtering, the final mapping population was composed of 304 recombinant progeny. 46,670 variable sites were identified between the parental strains that were collapsed into 4,943 haploblocks.

Cross-Species Amoeba Resistance QTL

The F_1 segregants generated from the Bt22 $\times$ Ftc555-1 cross exhibited a diverse response to amoeba predation (mean of predation area 23.46 cm^2 and SD 14.99 cm^2). There is a substantial amount of transgressive segregation – 16.9% of the segregants exhibited resistance higher than Ftc555-1, and 38.4% of segregants exhibited lower resistance than Bt22 (Fig. 2B). Substantial transgressive segregation suggests that epistatic interactions between parental alleles contribute to both increased and decreased resistance beyond the parental phenotypes. Segregant genotypes and phenotypes were combined to carry out QTL mapping based on a marker regression approach [47]. This QTL analysis revealed that genetic variation for amoeba resistance in the mapping population is dominated by a single, major effect locus on chromosome 8 (Fig. 3A). Segregants with Bt22 haplotypes at the chromosome 8 QTL peak exhibited significantly larger zones of amoeba clearance than those offspring with the Ftc555-1 haplotype (Fig. 3B). The QTL on chro-

mosome 8 explains an astonishing 62% of variation in amoeba resistance.

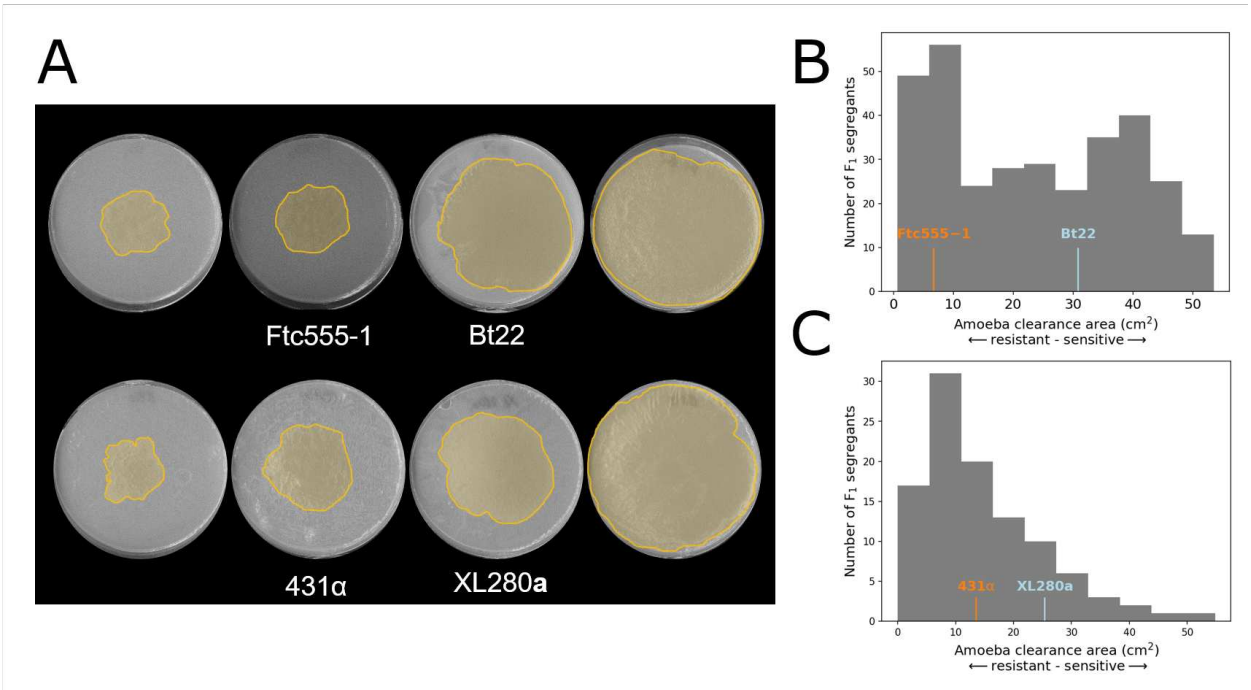

Figure 2: **Phenotypic variation in amoeba resistance in mapping populations derived from both *C. neoformans* and *C. deneoformans* crosses. A.** Representative images of plates from amoeba resistance assays. On the plates, the area consumed by amoeba are highlighted in yellow. Parental strains are shown in the middle panels, and transgressive segregants are on the left and right. **B.** A histogram displaying amoeba resistance of segregants in the *C. neoformans* cross. The x-axis represents the amoeba clearance area. Phenotypes of the two parental strains are indicated in orange (Ftc555-1) and blue (Bt22). **C.** A histogram of the *C. deneoformans* F_1 progeny amoeba phenotypes. Phenotypes of the two parental strains are indicated in orange (431) and blue (XL280)

To determine if there are similarities in the genetic architecture of amoeba resistance between closely related pathogenic species of *Cryptococcus*, we carried out a similar analysis using a mapping population derived from a *C. deneoformans* cross described in [47]. This cross, between strains XL280**a** and 431α, consists of 90 recombinant progeny. XL280**a** and 431α have only modest differences in amoeba resistance, but similar to the findings in *C. neoformans*, the *C. deneoformans* offspring exhibited a high degree of transgressive segregation for this trait. 15.4% of offspring displayed negative transgressive segregation (segregants with lower amoeba resistance than XL280**a**), 54.8% positive transgressive segregation (segregants with lower amoeba resistance than 431α), and 29.8% non-transgressive (Fig. 2A,D). QTL analysis of this population identified a significant peak on chromosome 7 that explains 23% of the variance of amoeba resistance (Fig. 3C). Progeny with the 431α allele on chromosome 7 have a higher average resistance to amoeba (Fig. 3D). By examination of the genes under the QTL peak on chromosome 7, this region was found to be orthologous to the *C. neoformans* QTL peak on chromosome 8. These two regions share 82% nucleotide sequence identity and conserved synteny (Fig. 3E), suggesting there

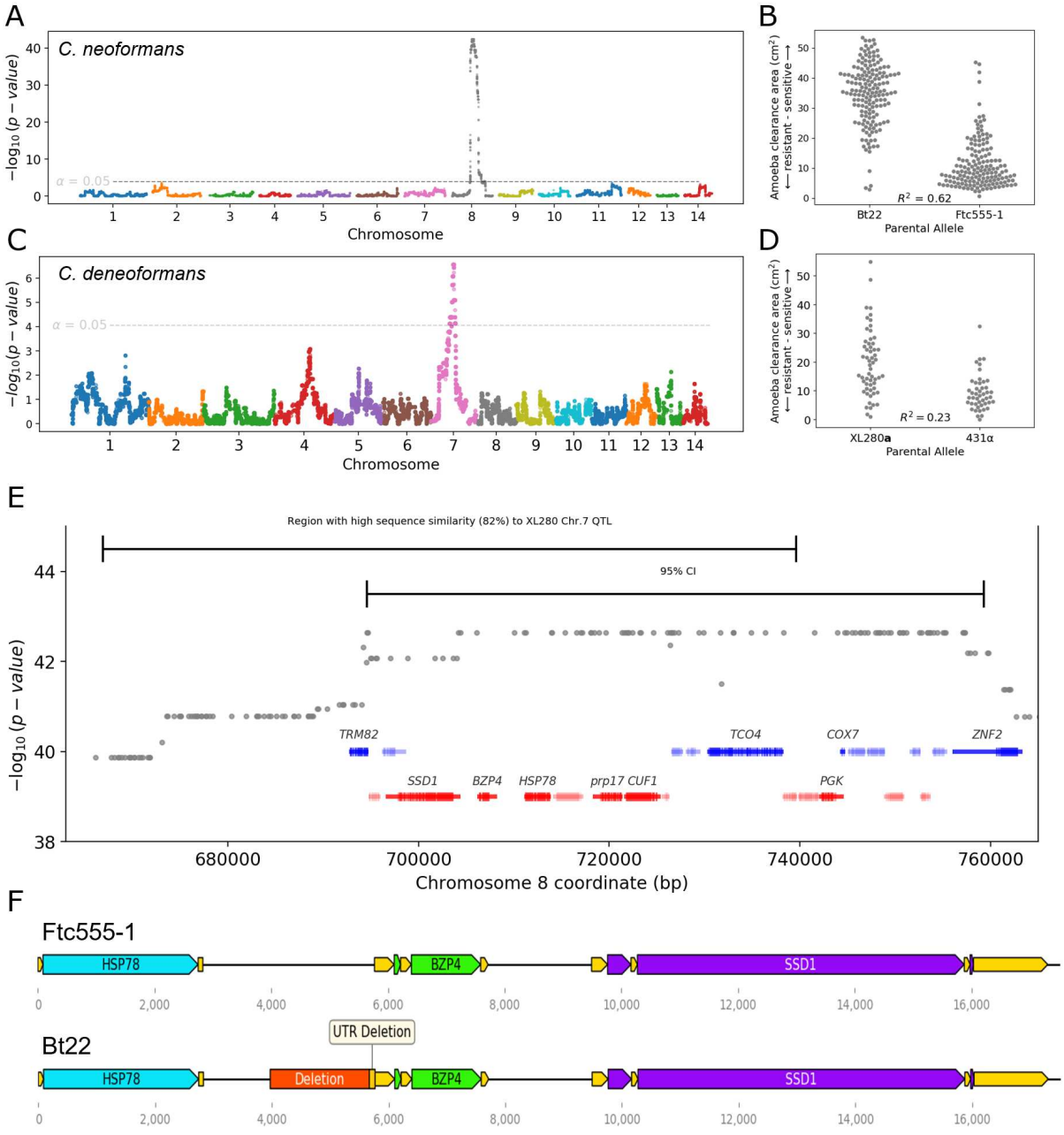

Figure 3: **Amoeba resistance QTL for *C. neoformans* and *C. deneoformans*. A.** Manhattan plot representing the association between genotype and amoeba resistance in the *C. neoformans* mapping populations. The dotted line indicates the significance threshold determined by permutation. **B.** Distributions of segregant phenotypes associated with the QTL peak on chromosome 8 for *C. neoformans*. The x-axis represents allelic state at the QTL peak. This peak explains 62% of the amoeba resistance variation (R^2). **C.** Manhattan plot for amoeba resistance in the *C. deneoformans* mapping population. This peak explains 62% of the amoeba resistance variation (R^2). **D.** Segregant phenotypes by chromosome 7 genotype for *C. deneoformans*. **E.** A magnified view of the 95% confidence interval of the *C. neoformans* QTL for amoeba resistance. Barred lines at the top are the 95% confidence intervals for the *C. deneoformans* and *C. neoformans* amoeba resistance QTL. **F.** Gene diagrams for the region around the *BZP4* gene for Ftc555-1 and Bt22. UTRs are shown in yellow.

are conserved genes required for amoeba resistance within the *Cryptococcus* species complex.

Identification of an Amoeba Resistance Gene

To identify candidate causal variants for the QTL region on chromosome 8 in the *C. neoformans* cross, we analyzed the predicted effect of nucleotide sequence differences on annotated features in this region (Table S1). 25 genes were within the identified 64 kb region that comprises the 95% confidence interval for this QTL. Ten of these genes have an annotated function or have homology to annotated genes in other fungal species. Across all of the genes in the QTL region, 31 synonymous mutations, 29 non-synonymous mutations, and two indels were identified. The two indels both result in nonsense mutations but these genes have no characterized function, no known gene deletion phenotype, and the mutations are in the opposite direction than we would predict for the QTL effect (i.e. they were present in the resistant strain, suggesting gene deletion would improve resistance). Further characterization of non-coding regions in the QTL region led to the identification of a large sequence difference between Bt22 and Ftc555-1, a 1789 bp deletion occurs in the Bt22 background in the intergenic region between the *BZP4* and *HSP78* genes. The Bt22 variant truncates 100 bp of the annotated *BZP4* 5' UTR and 1689 bp further upstream (Fig. 3F).

With *C. neoformans* phylogenetic data and short-read sequence data from [48], a strain was identified, Bt45, that is nearly genetically identical to Bt22 (~200 SNP differences) but does not share the deletion upstream of *BZP4* (Fig. 4A). The amoeba resistance of Bt45 and it was found to exhibit significantly greater resistance than Bt22 (pairwise t-test $P < 0.0005$), though not to the level observed for Ftc555-1 (Fig. 4B). This comparison between these two nearly genetically identical strains is analogous to an "allele exchange" experiment and provides strong evidence that the non-coding variant identified upstream of *BZP4* is the likely causal variant underlying the Chromosome 8 QTL.

To provide further evidence of *BZP4*'s contribution to amoeba resistance, CRISPR-Cas9 editing was utilized to delete *BZP4* in the Ftc555-1 background [49, 50]. Two independent *bzp4*Δ mutants were isolated and their amoeba resistance phenotypes were assessed. Both mutants exhibited a significant reduction in amoeba resistance (pairwise t-test $P < 0.0005$) and melanization (Fig. 4B, S3).

In sum, multiple lines of evidence suggest that the 1789 bp deletion we identified upstream of *BZP4* is the causal variant for the large effect amoeba resistance QTL we identified on chromosome 8. For the sake of conciseness, in the text that follows the two allelic states at this locus are referred to as $BZP4^{B}$ (Bt22 allele) and $BZP4^{F}$ (Ftc555-1 allele).

BZP4 is a pleiotropic QTG for Amoeba Resistance and Melanization

BZP4 is a transcription factor that has been shown to play a role in regulation of the melanin synthesis pathway under nutrient deprivation conditions [51]. Variation at the *BZP4* locus was previously

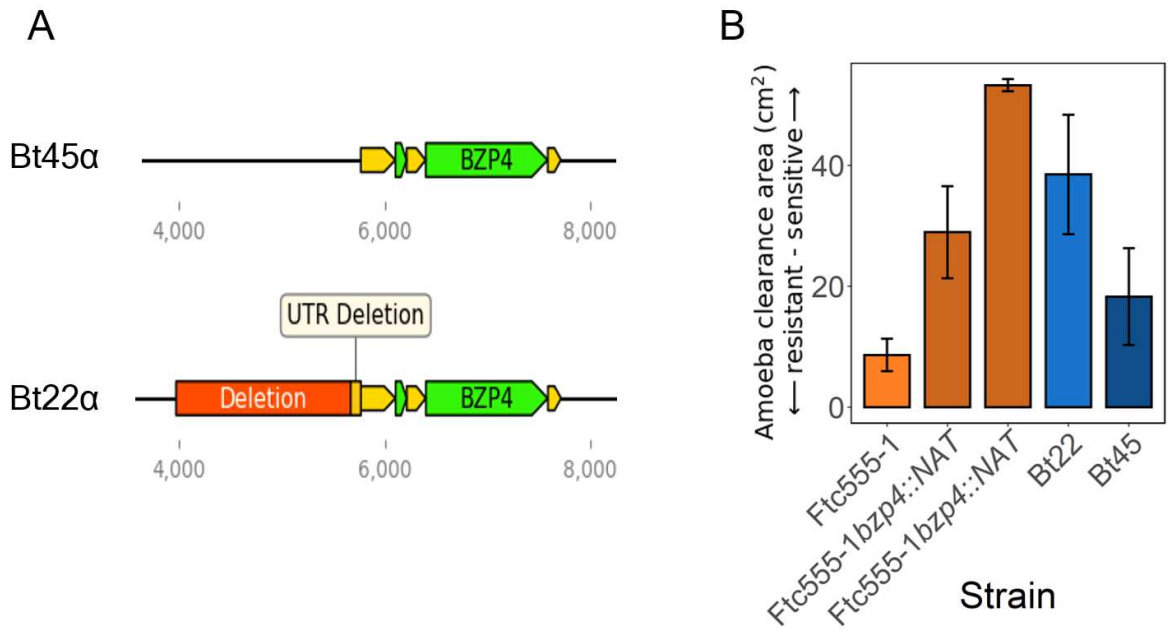

Figure 4: **Disruption of *BZP4* reduces amoeba resistance. A.** Models of the genomic regions surrounding *BZP4* in Bt22 and Bt45. **B.** Amoeba resistance assay for two independent gene deletions of *BZP4* in the Ftc555-1 background and a closely related strain of Bt22, Bt45. Bars are colored for comparison between closely related strains. The x-axis represents the strain tested. The y-axis represents the area amoeba consumed.

identified in a genome-wide association study (GWAS) for melanization [48]. In that study, *bzp4* loss-of-function mutations, found exclusively in clinical isolates, were shown to correlate with reduced melanization. A later study found that decreased expression of *BZP4* is correlated with decreased melanization in VNI clinical isolates [52].

Based on the role of *BZP4* in the regulation of melanin synthesis, we reasoned that the *BZP4* variant identified in the amoeba resistance mapping might also result in differences in the ability to produce melanin. While neither of the parent strains in the cross lacks melanin, Bt22 exhibits less melanin pigmentation than Ftc555-1 when grown under the same inducting conditions (Fig. 5A). The *C. neoformans* mapping population was assayed for the ability to produce melanin when grown on L-DOPA plates. Segregants in the cross ranged from completely white (devoid of melanin) to a deep ebony color accompanied by melanin leaking into the surrounding media (Fig. 5A). Across the segragants, 23.45% of the segregants displayed positive transgressive segregation (more melanized than Ftc555-1) while 24.43% displayed negative transgressive segregation (less melanized than Bt22). When the joint distribution of amoeba resistance and melaninization phenotypes among the offspring was assessed, a positive but non-linear relationship was observed (Fig. 5D).

QTL mapping based on the melanization phenotypes identified a major peak on chromosome 8 nearly identical in location to the QTL for amoeba resistance (Fig. 5C). This QTL explains a remarkable 50.2% of the phenotypic variation for melanization (Fig. 5B). Based on the similarity of the QTL for amoeba resistance and melanization (Fig. 5C), as well as the previously demonstrated role of *BZP4* in the regulation of melanin synthesis, we propose that the non-coding deletion upstream of *BZP4* has pleiotropic effects on both of these traits.

In contrast to the findings in *C. neoformans*, the chromosome 7 QTL for amoeba resistance in the *C. deneoformans* cross does not appear to have a pleiotropic effect on melanization. Instead, a nonsense mutation in the gene *RIC8* is primarily responsible for variation in melanization for this cross as described in an earlier study from our research groups [47].

To test whether the relationship observed between amoeba resistance and melanization in our *C. neoformans* mapping population holds more broadly, we again employed the genetically diverse collection of *C. neoformans* strains described above. This collection was supplemented with additional strains that have predicted *BZP4* loss-of-function mutations, and amoeba resistance and melanization for each isolate was measured. All strains, including those with predicted *BZP4* loss-of-function mutations, are capable of producing melanin given sufficient incubation time (Fig. S3). However, large differences in the rate of melanization between strains were observed and images taken at two days of growth as a measure of the variation were used. When comparing amoeba resistance and melanization across the diverse strain set, the reference strain H99 is notable as an outlier in terms of the bivariate relationship among these traits (Fig. S4). With H99 excluded, there is a strong linear relationship between amoeba resistance and melanization (R^2 = 0.58) (Fig. 5E). A notable trend among strains with predicted *BZP4* loss-of-function mutations is that those that melanize more readily (Bt103 and Bt102) are more resistant to amoeba than those that melanize

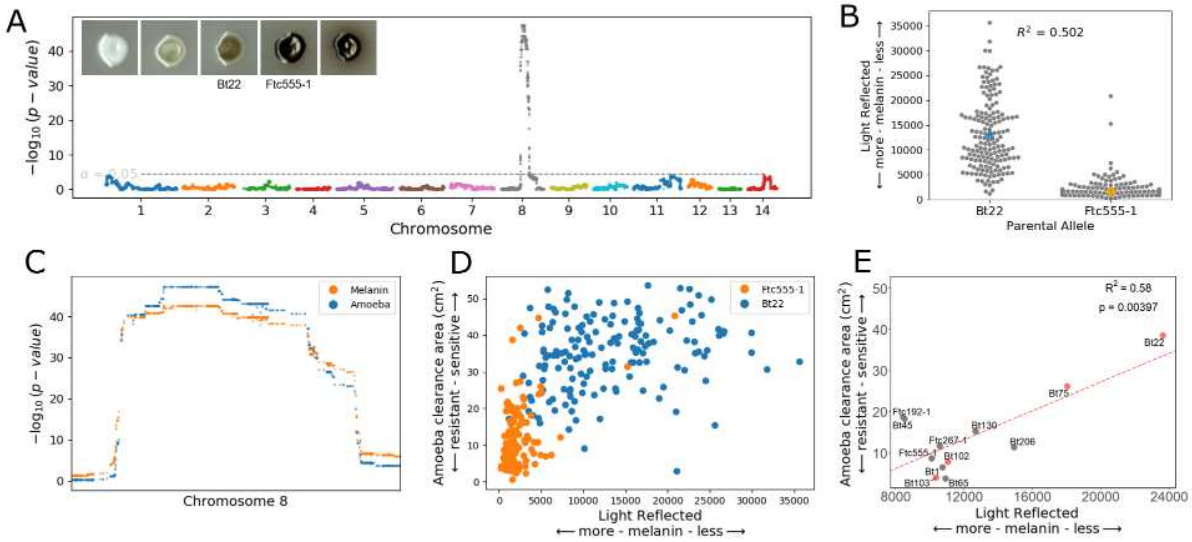

Figure 5: **Melanization and amoeba resistance share the same QTL. A.** Manhattan plot representing the association between genotype and melanization in the *C. neoformans* plot. The y-axis represents the strength of the association between genotype and light reflected (the degree of melanization). The x-axis represents the genomic location of the haploblocks used in the associations. The dotted line represents a significance threshold determined by a permutation test. Representative images of parents and segregants on L-DOPA media are also included. Each colony is from the randomized plates employed for QTL mapping. Images are brightened 30% to better display the difference in pigmentation. **B.** Segregant phenotypes at the maximum significance value of the QTL on chromosome 8. The x-axis represents the segregant allele at the maximum significance of the QTL. The y-axis represents the light reflected off of the colony when melanized. Parental strains are indicated in orange (Ftc555-1) and blue (Bt22). **C.** A magnified view of the chromosome 8 QTL peaks for amoeba resistance and melanization illustrating the QTL overlap. **D.** Plot comparing amoeba resistance and melanization phenotypes. The x-axis represents melanization and the x-axis represents amoeba resistance. Each dot represents a single segregant. Segregants are colored by their allele at the chromosome 8 QTL. **E.** Correlation between amoeba resistance and melanization in natural isolates, with the strain H99 removed. $p<0.005$

slowly (Bt22 and Bt75) (Fig. 5E).

Gene Expression Differences Associated with *BZP4* Allelic Variation

Since the *BZP4* allele identified involves a deletion of a large upstream non-coding region, we hypothesized that the phenotypic effects of this allele are mediated by a reduction in the expression of the *BZP4* gene, with consequent effects on the downstream targets of this transcription factor. To test this hypothesis, gene expression was profiled with RNAseq. Using six offspring with each *BZP4* genotype (6 for Bt22 and 6 for Ftc555-1; 12 strains in total) transcriptional responses when grown on V8 medium were compared with or without the addition of amoeba.

BZP4 was significantly differentially expressed between strains with the $BZP4^B$ and $BZP4^F$ alleles, in both amoeba and non-amoeba conditions (Fig. 6A, B). $BZP4^B$ strains exhibited an average 1.83-Log_2 fold decrease in expression relative to $BZP4^F$ strains when co-cultured with amoeba and a 2.06-Log_2 fold decrease when amoeba were absent (Fig. 6A). No other gene within the chromosome 8 QTL showed statistically significant differences in expression. While there are differences in *BZP4* expression between genotypes, no significant change in the expression of *BZP4* was observed between control and amoeba conditions (Fig. 6A). This suggests that the effect of the *BZP4* allelic differences identified is not specific to the amoeba challenge conditions of our assay.

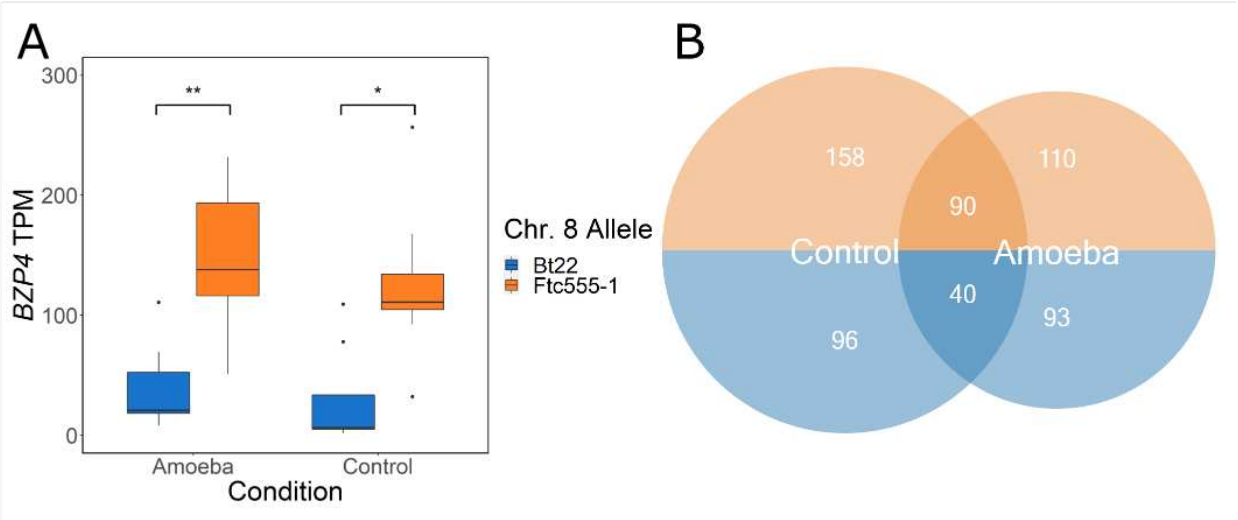

Figure 6: ***BZP4* expression differs significantly between genotypes. A.** Boxplots representing the difference in transcript abundance between conditions in transcript per million (TPM) with each parental allele under the chromosome 8 QTL. The y-axis represents the total transcript counts. Boxplots are colored by parental allele. Significance is determined by ANOVA. "**" $p < 0.005$; "*" $p < 0.05$ **B.** A Venn Diagram displaying the number of genes with increased and decreased expression for amoeba and control conditions based on the parental allele. Genes with decreased expression are colored in orange and those with increased expression are colored in blue.

Given that *BZP4* was identified as a candidate QTG for melanization, and the transcription factor it encodes has been previously implicated in the regulation of melanin synthesis genes,

we predicted that such genes would also exhibit differences in expression as a function of *BZP4* genotype. Contrary to this prediction, we found that no major melanin synthesis genes were significantly differentially expressed between genotypes (when filtered for biological significance by fold change), when measured on the V8 growth media used in the amoeba experiments (Fig. S3).

Investigating genome wide expression differences, 587 genes exhibited a greater than 2-fold difference between genotypes in either amoeba and control conditions. Of the 589 differentially expressed genes, 130 are shared between conditions, 254 are specific to the control conditions, and 203 are amoeba specific. Using GO term analysis for the 90 shared gene that have increased expression when *BZP4* expression is reduced, we find transmembrane transporter activity, oxidoreductase activity, and transition metal ion binding to increase in activity with reduced *BZP4* expression. Interestingly, there is a paucity of GO predictions for the 40 shared genes that are decreased in expression with reduced *BZP4* expression, as many of the genes are hypothetical or poorly characterized. The number of genes that have an inverse transcriptional relationship with *BZP4* expression indicates a role in gene repression. GO terms specific to amoeba conditions further include transmembrane transporter activity and oxidoreductase activity.

Epistatic QTLs for Amoeba Resistance and Melanization

While the pleiotropic chromosome 8 QTL we identified in the *C. neoformans* cross explains a large portion of variation for both amoeba resistance and melanization, both traits show continuous rather than bimodal distributions and there is a large degree of transgressive segregation. These observations suggested that there are likely additional alleles, perhaps interacting epistatically with the major effect allele on chromosome 8, that contribute to phenotypic differences in both of these traits. To test for epistatic interactions, our mapping population was subdivided based on the chromosome 8 genotype, and reanalyzed the mapping models for each subpopulation (Fig S2). For amoeba resistance, a single epistatic QTL was found on chromosome 5, exclusive to the segregants with the Ftc555-1a allele on chromosome 8 (Fig S2A). This epistatic chromosome 5 QTL explains 19% of the variation within that subgroup and it increases the overall variance explained for amoeba resistance to 64%. We identified two epistatic QTL for melanization, one in the segregants that have the Bt22 allele on chromosome 8 and the second in those that have the Ftc555-1 allele (Fig S2B). The epistatic QTL in the Bt22 background is found on chromosome 1 and explains 26% of the variation within that subgroup. The epistatic allele in the Ftc555-1 background occurs on chromosome 7 and accounts for a more modest 7.8% of variance. With these epistatic interactions included, the variance in melanization explained by all of the QTL identified increases to 56.4%. Evidence of epistasis for amoeba resistance and melanization highlights the importance of strain background and the impact of individual allelic differences on traits of interest.

Comparing Amoeba Resistance and Virulence

The accidental pathogen hypothesis is based on the similarities between amoeba and macrophage interactions with *Cryptococcus*. Both amoeba and macrophages employ similar methods of detecting, phagocytosing, and degrading fungal cells but the question remains: does survival when challenged with one phagocyte relate to success with the other? To answer this question, we measured the internal proliferation rate (IPR) in macrophages of progeny from the Bt22 $\times$ Ftc555-1 cross. F_1 Progeny were chosen to represent opposite extremes in terms of their amoeba resistance phenotypes. These low and high resistance strains were assayed alongside the parental strains. J774A.1 murine macrophages were infected with *C. neoformans* cells and the internal proliferation rate of yeast cells was measured using time lapse microscopy as described in the Methods. All F_1 progeny assayed, regardless of *BZP4* genotypes and amoeba resistance phenotypes, showed similar macrophage internal proliferation rates (Fig. 7A). Phagocytic index, another measure of yeast-macrophage interactions, also showed no association with *BZP4* allelic variation or amoeba resistance (Fig. S1). Thus, in contrast to the predictions of the accidental pathogen hypothesis, we do not observe a relationship between amoeba resistance alleles and survival in macrophages.

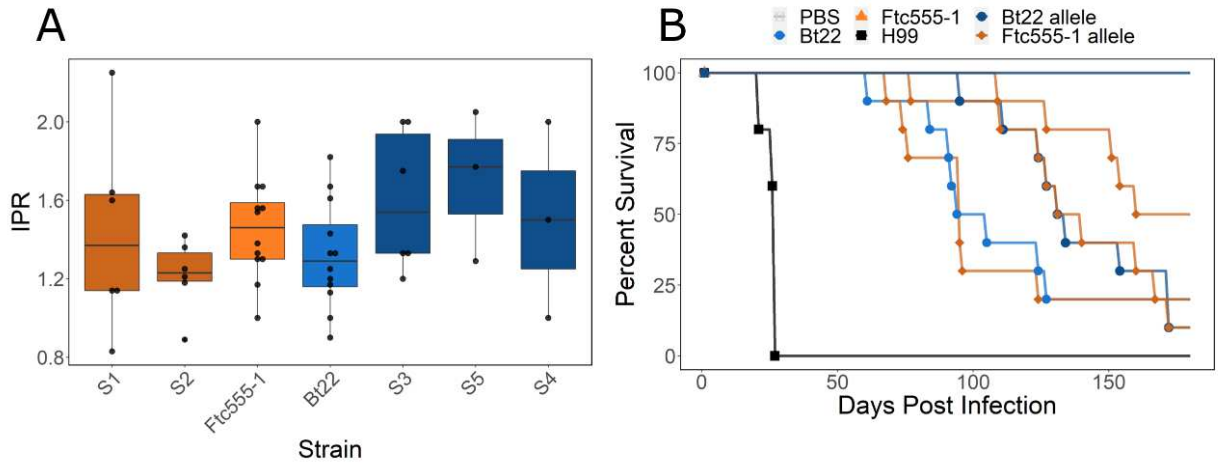

Figure 7: **Amoeba resistance and virulence tests do not correlate A.** Barplots representing the internal proliferation rate of parental strains and segregants. Boxplots are colored by the chromosome 8 allele. Orange boxes have the Ftc555-1 allele and blue have the Bt22 allele, darker colors indicate segregants. Dots represent individual measurements. Strains are oriented in rank order of amoeba resistance (highest to lowest resistance). Significance determined by ANOVA p = 0.29 F = 1.28. **B.** Survival curves for animals infected with the parental strains and a group of F_1 segregants. H99 is in black, Ftc555-1 is in orange, and Bt22 is in blue. Segregant curves are colored by parental allele under the chromosome 8 QTL, dark blue represents the Bt22 allele and darker orange represents the Ftc555-1 allele.

To explore the relationship between amoeba resistance and the ability to cause disease in animal models, an equal number of 4-5 week old male and female A/J mice were intranassally infected with F_1 progeny from the *C. neoformans* cross, the parental strains, and the reference

strain H99. Survival was monitored for a period of 179 days, with animals sacrificed based on disease progression symptoms (Fig. 7B). Though this analysis involve only a modest number of strains, we observed no relationship between *BZP4* genotype and virulence in mice. The virulence of the parental strains, Bt22 and Ftc555-1, is the opposite of their amoeba resistance phenotypes. Bt22, which exhibits low resistance to amoeba predation, has modest virulence with a time to 50% lethality (LT50) of ~92 days. This is in stark contrast to Ftc555-1, which is highly resistant to amoeba, but is completely avirulent in the mouse model of infection employed. The reference strain, H99, is strongly virulent in mice (LT50 ~21 days) but has very low amoeba resistance. Furthermore, we detected no association between LT50 estimated from murine survival curves and the *BZP4* genotype of a small number of segregants (Fig. 7B).

Finding a lack of correlation between amoeba resistance and virulence for strains from our mapping population, the analyses was broadened to include an additional nine, genotypically diverse *C. neoformans* strains. Using the same intranasal murine infection model described above, we found that virulence was highly variable among strains, but again found no correlation between amoeba resistance and LT50 measures of mouse survival (Fig. S5) [53].

Discussion

Our findings provide novel insights into the genetic architecture of fungal-amoebal interactions and the potential impact of selection for amoeba resistance on *Cryptococcus* virulence. Using QTL mapping, we identified a transcription factor, *BZP4*, that is important for *C. neoformans* survival in the presence of amoeba. This gene also affects melanization, a classical virulence trait that is considered important for the pathogenic abilities of *Cryptococcus* [54, 55, 56, 32]. Despite its role in mediating interactions with amoeba and the production of melanin, allelic variation at *BZP4* is not predictive of proliferation rates in macrophages or virulence in mouse models of infection. This suggests that the relationship between resistance to amoeba and virulence potential may be more complex than the accidental pathogen hypothesis predicts.

Another striking outcome of our study is the discovery of an amoeba resistance QTL in homologous genomic regions for both *C. neoformans* and *C. deneoformans*. Cross species QTLs are rare, but they have been found for drought resistance between species of legume [57], a cardiovascular disease marker between humans and baboons [58], and gravitropism in corn and *Arabidopsis* [59]. Our study marks the first detection of cross species QTL in fungi and it suggests that the amoeba survival mechanisms discovered may be conserved between different pathogenic species of *Cryptococcus*. We have not, as yet, identified the specific causal variant for the amoeba QTL in *C. deneoformans*, though non-coding variants in the vicinity of *BZP4* are among the top candidates we intend to pursue in future work.

We were initially surprised to find a single QTL for amoeba resistance and melanization in *C. neoformans*. The continuous distribution of amoeba resistance and melanization in the F_1 progeny implied more complex regulation than a single QTL would explain. Continuous traits are often gov-

erned by epistatic interactions between genes leading to the consideration of loci-loci interactions when discussing the effect of a QTL [60, 61]. Prior studies from our group have uncovered complex epistatic relationships that govern virulence phenotypes utilizing QTL mapping in *Cryptococcus* [47, 62]. Using the same techniques, we discovered an additional QTL for amoeba resistance and two additional QTL for melanization. Future work will detail the genes that underly these loci and their epistatic interactions. These additional epistatic QTL are indicative of the polygenic nature of stress response regulation. They also provide insight into the impact of strain background on the connection between individual loci and phenotype.

The importance of strain background prompted further investigation into the results of a prior GWAS analysis that implicated *BZP4* loss-of-function mutations with reduced melanization capacity [48]. In our re-analysis of the large set of sequenced genomes from this study, we noted that *BZP4* loss of function is found only in strains isolated in clinical settings. This corroborates a similar finding that reduced expression of *BZP4* is unique to clinical strains [52]. Furthermore, each of the candidate *BZP4* loss-of-function mutations we identified appears to be both independent and recent based on comparison to closely related strains. These observations lead us to speculate that *BZP4* loss-of-function mutations may actually be advantageous during human infection. If this is the case, this would further call into question the connection between amoeba resistance and virulence.

Our findings share a mix of both similarities and differences to a recent study by Fu et al. that employed experimental evolution to identify phenotypes and mutations selected for during *Cryptococcus* co-culture with amoeba [63]. A reduction in melanization was one of the phenotypic changes they observed that was most consistent across the three genetic backgrounds studied. This is in contrast to our findings, where we found that melanization was correlated with *higher* resistance to amoeba. However, similar to what we report here, their study failed to detect an association between amoeba resistance and macrophage challenge or virulence in mice. A particularly interesting genotypic change that Fu et al. identified in three independently evolved populations, derived from the H99 strain background, was duplications of chromosome 8. In light of our current study, the effect of a duplication of *BZP4*, which is located on chromosome 8, should be noted as a potential additional positive effect on amoeba resistance.

In our *C. neoformans* mapping population, we observed a positive, but non-linear relationship, between amoeba resistance and melanization, and *BZP4* is a candidate QTG for both of these traits. This raises the question, ”Do differences in melanization mediate variation in amoeba resistance?” Several lines of evidence suggest that this may only be part of the story. We found that *BZP4* is differentially expressed, as a function of *BZP4* genotype, in both control and amoeba conditions. Bzp4 is a transcriptional activator of *LAC1*, the gene responsible for the enzyme laccase that catalyzes the reaction of dopamine to melanin in *Cryptococcus* [64]; however, *LAC1* expression, and the expression of other key genes in the melanin synthesis pathway, do not vary as a function of *BZP4* genotype in the V8 media conditions used to co-culture amoeba and *Cryptococcus*. In addition, we did not observe melanization of *Cryptococcus* on V8 media, regardless of the

presence or absence of amoeba. This is in contrast to our finding that amoeba resistance broadly correlates with melanization, and the observation that *BZP4* loss-of-function strains that rapidly melanize have increased amoeba resistance. This leads us to propose a model in which *BZP4* affects amoeba resistance through both melanin-dependant and melanin-independent mechanisms. Among the pathways by which *BZP4* could affect amoeba resistance beyond melanin synthesis, *BZP4* has been found to positively regulate thiol-dependent ubiquitinyl hydrolase activity and negatively regulate aldo/keto reductase activity [65]. Future studies that characterize the transcriptional targets of Bzp4, such as through ChIP-seq analysis, will be critical to test these alternate hypotheses and reconcile the relative contribution of melanin synthesis and other processes to amoeba resistance.

Our discovery of QTLs for amoeba resistance in homologous genomic regions in both *C. neoformans* and *C. deneoformans*, suggests that amoeba resistance mechanisms may be conserved in the *Cryptococcus* genus. If the transcription factor *BZP4* is a key element in mediating escape from amoeba, as the evidence supports, an interesting question is whether *BZP4* function is an absolute requirement. Two clinical isolates, Bt102 and Bt103, suggest that this is not the case. These strains have predicted *bzp4* loss-of-function mutations, but were highly resistant to killing by amoeba. This could be due to allelic variation acting either downstream of *BZP4* or in a pathway parallel to *BZP4* that also governs amoeba resistance. This further emphasizes the importance of strain background in understanding the broader implications of gene function.

In summary, the transcription factor Bzp4 is important for the survival of *Cryptococcus* when exposed to phagocytic amoebae. Despite the importance of *BZP4* in amoeba resistance, *BZP4* function is not correlated with survival in macrophages nor is it predictive of virulence in mice. Furthermore, *BZP4* function may be selected against in some clinical isolates of *Cryptococcus*, which would suggest that amoebae and mammalian hosts are competing, rather than complementary, selective environments. While interactions with amoebae cannot be ruled out as a contributing factor to the evolution of *Cryptococcus* virulence, our findings suggest that phagocytic amoebae and phagocytic immune cells, despite their many parallels, are distinct niches from the perspective of fungal survival.

Materials and methods

Strains, Laboratory Crosses and Isolation

All strains were maintained on yeast peptone dextrose (YPD) plates grown at 30°C for 48 hours from -80°C stocks. Overnight cultures for amoeba assays, melanin assays, and RNA isolation were made in liquid YPD at 30°C on a rotor drum. Melanization was assayed by growing strains on minimal media plates with L-DOPA (7.6 mM L-asparagine monohydrate, 5.6 mM glucose, 10 mM MgSO4, 0.5 mM 3,4-dihydroxy-L-phenylalanine, 0.3 mM thiamine–HCl, and 20 nM biotin) for 72 hours. Plates were then scanned on an Epson Expression XL Flatbed Scanner in reflective mode at 300 dpi. ImageJ was used to calculate greyscale intensity of the colonies. Each sample was measured in triplicate.

Amoeba Resistance Assay

C. neoformans and *C. deneoformans* strains were grown overnight in 3 mL of liquid YPD on a roller drum before being diluted down to OD_{600} 0.6. 100 µL of diluted culture was spread on solid V8 media petri dishes using glass beads. Plates were grown at 30°C for 60 hours before being removed from the incubator. *Acanthamoeba castellanii* (ATCC 30234) were grown in ATCC 712 in a 75 mL tissue culture flask. Amoeba were harvested, between passage 5 and 15, from flasks and suspended at a concentration of 10^6 cells/mL before 50 µL of amoeba culture were pipetted onto the center of the *Cryptococcus* lawn. Plates were allowed to dry at room temperature on the bench top for 10 minutes and then placed in a 25°C incubator for 12 - 18 days. Measurements were taken at days 1, 12, and 18. Area of clearance was calculated by subtracting the day 1 measurement from the final day measurement as the day 1 measurement represented the initial spread of the amoeba culture on the plates. Two final time points were used (12 and 18 days) based on amoeba replication rate and activity. Rank order of amoeba affect was conserved between days 12 and 18.

Spore Dissection

Meiotic progeny were recovered by microdissection of random basidiospores as previously described [66]. Briefly, cells from the two parental strains were each resuspended in sterile water to a density of OD_{600}=1.0. Equal volumes of cell suspensions were mixed, and 5 μL of the mixture, as well as the two parental strains (serving as negative controls of mating), were spotted onto MS solid medium. The MS plates were incubated in the dark at room temperature (23°C for two weeks, at which time robust hyphae, basidia, and basidiospore chains were produced by the spots from the mixture of the two parental strains. Basidiospores from a large number of basidia in one location along the edge of the mating spot were picked directly from the MS plates using the needle of a dissection microscope each time, then transferred and separated onto YPD solid medium. To reduce the chances of sampling clones from the same basidia, we only separated limited numbers

of basidiospores from one location (<5%), and sampled multiple locations, as well as from multiple mating spots.

DNA extraction, Library Preparation, and Sequencing

DNA was extracted with MasterPure Yeast DNA Purification kit and cleaned up the Zymo Research Genomic Clean and Concentrator kit (following manufacturer's instructions) followed by quantification with PicoGreen. After quantifying the DNA with PicoGreen, samples were prepped for genomic sequencing using seqWell's plexWell 96 kit to prepare the libraries. Briefly, samples were individually bar-coded in sets of 96 using randomly inserted transposons, pooled, and then purified. Next, each pooled sample was bar-coded, enriched, and finally size-selected purified. Libraries were sequenced at Duke University's Sequencing and Genomic Technologies Facility on the NovaSeq 6000 S-Prime with 150 basepair paired end reads. Reads were aligned to the H99 *C. neoformans* reference genome using BWA. Variant calling was carried out using SAMtools and Freebayes.

Segregants Filtering and SNP Filtering

Segregants were filtered to remove aneuploidy and clonality described in detail in [67]. Of the original 384 segregants we were left with 304 after filtering. Variant sites were filtered based on read depth, allelic read depth ratio, quality scores, and minor allele frequency as described in [47]. Total number of bi-allelic variant sites prior to filtering was 59,430 that were reduced down to 46,670 after filtering.

QTL Mapping

he 46,670 genetic variants were combined into 4,943 haploblocks, defined by linkage, using methods described previously by Roth *et al.* [47]. For association testing of amoeba resistance and melanization, a Mann-Whitney U test was used across these 4,943 haploblocks to associate phenotype and genotype, coding the Bt22 and Ftc555-1 genotypes as zero and one respectively. The -log10 (p-value) from the Mann-Whitney U tests was monitored to identify QTL and 95% confidence intervals were calculated using permutation testing, a thousand times with replacement [68].

Permutation Testing

Permutation testing was carried out as described in [69] and [47] for establishing significance thresholds for QTL mapping. A thousand permutations were used for the melanin and amoeba phenotypes. Random assignments of genotype and phenotpe were held constant for every condition tested to preserve autocorrelation between phenotypes. The 95^{th} percentile of the permuted null distribution were used as the threshold for significance.

RNA Isolation and Sequencing

12 segregants and duplicates of the parental strains were used for the analyses comprising 16 individual samples. Samples were grown overnight in liquid YPD on a rollerdrum and were added to V8 petri dishes. V8 cultures were grown at 30°C for 60 hours. Amoeba cultures were collected and suspended at a concentration of 1×10^6 cells/mL. 450 µL of amoeba culture was added to the center of the *Cryptococcus* lawn with slight agitation to aid in the spread of the culture. Plates were allowed to dry on the benchtop for 30 minutes before being incubated at 25°C for 48 hours. A consistent area of 30 cm^2 was cut from the plates and then scraped to collect cells. Collected cells were resuspended in 1 mL of PBS and were placed in dry ice for 10 minutes. Samples were then lyophilized for 12 - 18 hours. Whole RNA was extracted using the RNAeasy Plant Mini Kit (Qiagen 74904).

Control samples did not have amoeba added to them, but were handled in a similar fashion in every other aspect of the protocol.

Libraries were prepared and sequenced by the Duke sequencing core using the Illumina NextSeq 500 High Output Kit producing 150-basepair paired end reads.

RNAseq Analysis

Reads were aligned using the CNA3 of H99 *C. neoformans* var. grubii (accession GCA_000149245.3). from the Ensemble Fungi database. Reads were aligned using Kallisto.

Analysis of RNA sequences was performed using Deseq2 in R. Briefly, transcript abundance was normalized using a built in median of ratios method. Samples were normalized based on condition (amobea or control). GO term analysis was performed using the fungidb GeneByLocusTag tool.

Tissue Culture

The J774A.1 macrophage cell line was cultured in T-75 flasks [Fisher Scientific] in Dulbecco's Modified Eagle medium, low glucose (DMEM) [Sigma-Aldrich], supplemented with 10% live fetal bovine serum (FBS) [Sigma-Aldrich], 2mM L-glutamine [Sigma-Aldrich], and 1% Penicillin and Streptomycin solution [Sigma-Aldrich] at 37°C and 5% CO^2.

Phagocytosis Assay

To measure the phagocytosis of various *Cryptococcus* segregants by macrophages, J774A.1 cells were seeded at a density of 1x10^5 cells per well of a 24-well plate [Greiner Bio-One], then incubated overnight at 37°C and 5% CO^2. At the same time, an overnight culture of *C. neoformans* parental strains or segregants was set up by picking a fungal colony from YPD agar plates (50g/L YPD broth powder [Sigma-Aldrich], 2% Agar [MP Biomedical]) and resuspending it in 3mL liquid YPD broth

(50 g/L YPD broth powder [Sigma-Aldrich]). The culture was then incubated at 25°C overnight under constant rotation (20rpm).

On the day of the assay, macrophages were activated using 150ng/mL phorbol 12-myristate 13-acetate (PMA) [Sigma-Aldrich] for 1 hour at 37°C. PMA stimulation was performed in serum-free media to eliminate the contribution of complement proteins during phagocytosis. To prepare *C. neoformans* for infection, overnight *C. neoformans* cultures were washed two times in 1X PBS, counted using a hemacytometer, and fungi was incubated with macrophages at a multiplicity of infection (MOI) of 10:1. The infection was allowed to take place for 2h at 37 °C and 5% CO^2. After 2 h infection, as much extracellular *Cryptococcus* as possible was washed off using 1X PBS.

Fluorescent Microscopy Imaging

The number of phagocytosed fungi was quantified from images from a fluorescent microscope. To distinguish between phagocytosed and extracellular *C. neoformans*, wells were treated with 10 µg/mL calcofluor white (CFW) [Sigma-Aldrich] for 10 mins at 37°C. The wells were washed again with PBS to remove residual CFW. Fluorescent microscopy images were acquired at 20X magnification using the Nikon Eclipse Ti inverted microscope [Nikon] fitted with the QICAM Fast 1394 camera [Hamamatsu]. Images were analysed using the Fiji image processing software [ImageJ]. To quantify the number of phagocytosed *Cryptococcus* from the resulting images, the total number of ingested *C. neoformans* was counted in 200 macrophages, then the values were applied to the following equation: ((number of phagocytosed *C. neoformans*/number of macrophages) $\times$100).

Intracellular Proliferation Rate Assay and Time-lapse Imaging

To investigate the intracellular proliferation rate (IPR) of *Cryptococcus* strains within macrophages, infected macrophages were captured at a regular interval over an extended period. Time-lapse imaging was performed by running the phagocytosis assay as usual, then after washing off extracellular *Cryptococcus* with 1X PBS, serum-free culture media was added back into the wells before imaging. Images were captured using the Nikon Eclipse Ti microscope at 20X magnification. Images were acquired every 5 minutes for 18 hours at 37 °C and 5% CO2.

The resulting video was analysed using Fiji [ImageJ] and IPR was determined by quantifying the total number of internalised fungi in 200 macrophages at the 'first frame' (time point 0 (T0)) and 'last frame' (T10). The resulting values were used in the following equation: ((number of phagocytosed *C. neoformans*/number of macrophages) $\times$100). Next, the number of phagocytosed fungi at T10 was divided by the number of phagocytosed fungi at T0 to give the IPR (IPR = T10/T0).

Mouse Infections

Cryptococcus strains for inoculation were grown overnight in 5 ml of YPD broth at 30°C in a roller drum. Cells were pelleted by centrifugation and washed twice with sterile PBS. The cell pellet was

resuspended in PBS, diluted, and counted by hemocytometer. The final inoculum was adjusted to a cell density of 4 x 10^6 CFU/ml. Test groups consisting of five male and five female A/J mice aged 4-5 weeks were purchased from Jackson Labs (stock #000646) and infected via intranasal instillation. Mice were anesthetized using isoflurane administered with a calibrated vaporizer. 25 µl of the prepared inoculum was pipetted into the nares one drop at a time until the full volume containing 10^5 CFU was inhaled. Mice were observed until fully recovered from anesthesia. Following infection, mice were monitored daily for symptoms of disease progression including weight loss, labored breathing, lack of grooming, social isolation, and any signs of pain or distress. Mice were euthanized upon reaching humane endpoints according to guidelines set forth by Duke's Animal Care and Use Program. Survival curves were plotted using GraphPad Prism version 8 and analyzed using log-rank (Mantel-Cox) statistical test.

Ethics Statement

Animal experiments were performed under Duke protocol number A148-19-07, in accordance with guidance issued by Duke's Institutional Animal Care and Use Committee and the U.S. Animal Welfare Act. Animals were housed in facilities managed by veterinary staff with Duke Lab Animal Research (DLAR) and accredited by the Association for Assessment and Accreditation of Laboratory Animal Care (AAALAC).

References

[1] Brown SP, Cornforth DM, Mideo N. Evolution of virulence in opportunistic pathogens: Generalism, plasticity, and control. Trends in Microbiology. 2012;20:336–342. doi:10.1016/j.tim.2012.04.005.

[2] Lanzas C, Davies K, Erwin S, Dawson D. On modelling environmentally transmitted pathogens. Interface Focus. 2020;10. doi:10.1098/rsfs.2019.0056.

[3] Casadevall A. Evolution of intracellular pathogens. Annual Review of Microbiology. 2008;62:19–33. doi:10.1146/annurev.micro.61.080706.093305.

[4] Adiba S, Nizak C, van Baalen M, Denamur E, Depaulis F. From grazing resistance to pathogenesis: The coincidental evolution of virulence factors. PLoS ONE. 2010;5:1–10. doi:10.1371/journal.pone.0011882.

[5] Taylor-Mulneix DL, Soumana IH, Linz B, Harvill ET. Evolution of *Bordetellae* from environmental microbes to human respiratory pathogens: amoebae as a missing link. Frontiers in Cellular and Infection Microbiology. 2017;7:1–7. doi:10.3389/fcimb.2017.00510.

[6] Best A, Kwaik A. Evolution of the arsenal of *Legionella pneumophila* effectors To modulate protist hosts. mBio. 2018;9:1–16.

[7] Siddiqui R, Lakhundi S, Khan NA. Interactions of *Pseudomonas aeruginosa* and *Corynebacterium spp.* with non-phagocytic brain microvascular endothelial cells and phagocytic *Acadnthamoeba castellanii*. Parasitology Research. 2015;114:2349–2356. doi:10.1007/s00436-015-4432-0.

[8] Albuquerque P, Nicola AM, Magnabosco DAG, da Silveira Derengowski L, Crisóstomo LS, Xavier LCG, et al. A hidden battle in the dirt: Soil amoebae interactions with *Paracoccidioides spp*. PLoS Neglected Tropical Diseases. 2019;13. doi:10.1371/journal.pntd.0007742.

[9] Steenbergen JN, Shuman HA, Casadevall A. *Cryptococcus neoformans* interactions with amoebae suggest an explanation for its virulence and intracellular pathogenic strategy in macrophages. Proceedings of the National Academy of Sciences. 2001;98:15245–15250. doi:10.1073/pnas.261418798.

[10] Fan Y, Wang Y, Korfanty GA, Archer M, Xu J. Genome-wide association analysis for triazole resistance in *Aspergillus fumigatus*. Pathogens. 2021;10. doi:10.3390/pathogens10060701.

[11] Waeyenberghe LV, Baré J, Pasmans F, Claeys M, Bert W, Haesebrouck F, et al. Interaction of *Aspergillus fumigatus* conidia with *Acanthamoeba castellanii* parallels macrophage-fungus interactions. Environmental Microbiology Reports. 2013;5:819–824. doi:10.1111/1758-2229.12082.

[12] Yan L, Cerny RL, Cirillo JD. Evidence that Hsp90 is involved in the altered interactions of *Acanthamoeba* castellanii variants with bacteria. Eukaryotic Cell. 2004;3:567–578. doi:10.1128/EC.3.3.567-578.2004.

[13] Escoll P, Rolando M, Gomez-Valero L, Buchrieser C. In: Hilbi H, editor. From amoeba to macrophages: exploring the molecular mechanisms of *Legionella pneumophila* infection in both hosts. Berlin, Heidelberg: Springer Berlin Heidelberg; 2014. p. 1–34. Available from: https://doi.org/10.1007/82_2013_351.

[14] Davies B, Chattings LS, Edward SW. Superoxide generation during phagocytosis by *Acanthamoeba castellanii*: similarities to the respiratory burst of immune phagocytes. Journal of general microbiology. 1991; p. 705–710.

[15] German N, Doyscher D, Rensing C. Bacterial killing in macrophages and amoeba: Do they all use a brass dagger? Future Microbiology. 2013;8:1257–1264. doi:10.2217/fmb.13.100.

[16] Smith MD, Gu Y, Querol-Audí J, Vogan JM, Nitido A, Cate JHD. Human-like eukaryotic translation initiation factor 3 from *Neurospora crassa*. PLoS ONE. 2013;8. doi:10.1371/journal.pone.0078715.

[17] Casadevall A, Fu M, Guimaraes A, Albuquerque P. The 'Amoeboid Predator-Fungal Animal Virulence' Hypothesis. Journal of Fungi. 2019;5:10. doi:10.3390/jof5010010.

[18] Castellanii A. An amoeba found in culture of yeast: preliminary note. Journal of Tropical Medicine London. 1930;33:160.

[19] Ruiz A, Neilson JB, Bulmer GS. Control Of *Cryptococcus neoformans* In nature By biotic factors. Sabouraudia. 1982; p. 21–29.

[20] Rajasingham R, Smith RM, Park BJ, Jarvis JN, Govender NP, Chiller TM, et al. Global burden of disease of HIV-associated cryptococcal meningitis: an updated analysis. The Lancet Infectious Diseases. 2017;17:873–881. doi:10.1016/S1473-3099(17)30243-8.

[21] Siddiqui NAKR. Biology and pathogenesis of Acanthamoeba. Parasites Vectors. 2012;5:269–294.

[22] Brown GD, Denning DW, Gow NAR, Levitz SM, Netea MG, White TC. Hidden killers: Human fungal infections. Science Translational Medicine. 2012;4. doi:10.1126/scitranslmed.3004404.

[23] Voelz K, May RC. Cryptococcal interactions with the host immune system. Eukaryotic Cell. 2010;9:835–846. doi:10.1128/EC.00039-10.

[24] May RC, Stone NRH, Wiesner DL, Bicanic T, Nielsen K. *Cryptococcus*: From environmental saprophyte to global pathogen. Nature Reviews Microbiology. 2016;14:106–117. doi:10.1038/nrmicro.2015.6.

[25] Dromer F, Mathoulin-Pélissier S, Launay O, Lortholary O, Achard J, Chabasse D, et al. Determinants of disease presentation and outcome during cryptococcosis: The CryptoA/D study. PLoS Medicine. 2007;4:0297–0308. doi:10.1371/journal.pmed.0040021.

[26] O'Meara TR, Alspaugh JA. The *Cryptococcus neoformans* capsule: A sword and a shield. Clinical Microbiology Reviews. 2012;25:387–408. doi:10.1128/CMR.00001-12.

[27] Leon-Rodriguez CMD, Fu MS, Çorbali MO, Cordero RJB, Casadevall A. The capsule of *Cryptococcus neoformans* modulates phagosomal pH through its acidbase properties. mSphere. 2018;3:1–8. doi:10.1128/mSphere.00437-18.

[28] Zaragoza O, Chrisman CJ, Castelli MV, Frases S, Cuenca-Estrella M, Rodríguez-Tudela JL, et al. Capsule enlargement in *Cryptococcus neoformans* confers resistance to oxidative stress suggesting a mechanism for intracellular survival. Cellular Microbiology. 2008;10:2043–2057. doi:10.1111/j.1462-5822.2008.01186.x.Capsule.

[29] Leach MD, Cowen LE. Surviving the heat of the moment: A fungal pathogens perspective. PLoS Pathogens. 2013;9:1–4. doi:10.1371/journal.ppat.1003163.

[30] Findley K, Rodriguez-Carres M, Metin B, Kroiss J, Álvaro Fonseca, Vilgalys R, et al. Phylogeny and phenotypic characterization of pathogenic *Cryptococcus* species and closely related saprobic taxa in the tremellales. Eukaryotic Cell. 2009;8:353–361. doi:10.1128/EC.00373-08.

[31] Cordero ACRJ. Functions of fungal melanin beyond virulence. Fungal Biology Reviews. 2017;31:99–112. doi:10.1016/j.fbr.2016.12.003.Functions.

[32] Liu S, Youngchim S, Zamith-Miranda D, Nosanchuk JD. Fungal melanin and the mammalian immune system. Journal of Fungi. 2021;7:1–15. doi:10.3390/jof7040264.

[33] Djordjevic JT. Role of phospholipases in fungal fitness, pathogenicity, and drug development - lessons from *Cryptococcus neoformans*. Frontiers in Microbiology. 2010;1:1–13. doi:10.3389/fmicb.2010.00125.

[34] Cox GM, McDade HC, Chen SCA, Tucker SC, Gottfredsson M, Wright LC, et al. Extracellular phospholipase activity is a virulence factor for *Cryptococcus neoformans*. Molecular Microbiology. 2001;39:166–175. doi:10.1046/j.1365-2958.2001.02236.x.

[35] Cox GM, Mukherjee J, Cole GT, Casadevall A, Perfect JR. Urease as a virulence factor in experimental cryptococcosis. Infection and Immunity. 2000;68:443–448. doi:10.1128/IAI.68.2.443-448.2000.

[36] Kappaun K, Piovesan AR, Carlini CR, Ligabue-Braun R. Ureases: Historical aspects, catalytic, and non-catalytic properties – A review. Journal of Advanced Research. 2018;13:3–17. doi:10.1016/j.jare.2018.05.010.

[37] Chrisman CJ, Alvarez M, Casadevall A. Phagocytosis of *Cryptococcus neoformans* by, and nonlytic exocytosis from, *Acanthamoeba castellanii*. Applied and Environmental Microbiology. 2010;76:6056–6062. doi:10.1128/AEM.00812-10.

[38] da S Derengowski L, Paes HC, Albuquerque P, Tavares AHFP, Fernandes L, Silva-Pereira I, et al. The transcriptional response of *Cryptococcus neoformans* to ingestion by *Acanthamoeba castellanii* and macrophages provides insights into the evolutionary adaptation to the mammalian host. Eukaryotic Cell. 2013;12:761–774. doi:10.1128/EC.00073-13.

[39] Rizzo J, Albuquerque PC, Wolf JM, Nascimento R, Pereira MD, Nosanchuk JD, et al. Analysis of multiple components involved in the interaction between *Cryptococcus neoformans* and *Acanthamoeba castellanii*. Fungal Biology. 2017;121:602–614. doi:10.1016/j.funbio.2017.04.002.

[40] Steenbergen JN, Nosanchuk JD, Malliaris SD, Casadevall A. *Cryptococcus neoformans* virulence is enhanced after growth in the genetically malleable host Dictyostelium discoideum. Infection and Immunity. 2003;71:4862–4872. doi:10.1128/IAI.71.9.4862-4872.2003.

[41] Lin J, Idnurm A, Lin X. Morphology and its underlying genetic regulation impact the interaction between *Cryptococcus neoformans* and its hosts. Medical Mycology. 2015;53:493–504. doi:10.1093/mmy/myv012.

[42] Chen M, Xing Y, Lu A, Fang W, Sun B, Chen C, et al. Internalized *Cryptococcus neoformans* activates the canonical caspase-1 and the noncanonical caspase-8 inflammasomes. The Journal of Immunology. 2015;195:4962–4972. doi:10.4049/jimmunol.1500865.

[43] Perfect JR, Lang SDR, Durack DT. Chronic cryptococcal meningitis. A new experimental model in rabbits. American Journal of Pathology. 1980;101:177–193.

[44] Litvintseva AP, Marra RE, Nielsen K, Heitman J, Vilgalys R, Mitchell TG. Evidence of sexual recombination among *Cryptococcus neoformans* serotype A isolates in sub-Saharan Africa. Eukaryotic Cell. 2003;2:1162–1168. doi:10.1128/EC.2.6.1162-1168.2003.

[45] Nielsen K, Cox GM, Wang P, Toffaletti DL, Perfect JR, Heitman J. Sexual cycle of *Cryptococcus neoformans var. grubii* and virulence of congenic a and α isolates. Infection and Immunity. 2003;71:4831–4841. doi:10.1128/IAI.71.9.4831-4841.2003.

[46] Chen Y, Litvintseva AP, Frazzitta AE, Haverkamp MR, Wang L, Fang C, et al. Comparative analyses of clinical and environmental populations of *Cryptococcus neoformans* in Botswana. Molecular Ecology. 2015;24:3559–3571. doi:10.1111/mec.13260.

[47] Roth C, Murray D, Scott A, Fu C, Averette AF, Sun S, et al. Pleiotropy and epistasis within and between signaling pathways defines the genetic architecture of fungal virulence. PLoS Genetics. 2021;17:1–44. doi:10.1371/journal.pgen.1009313.

[48] Desjardins CA, Giamberardino C, Sykes S, Yu CH, Tenor J, Chen Y, et al. Population Genomics And The Evolution Of Virulence In The Fungal Pathogen *Cryptococcus neoformans*. Cold Springs Harbor Laboratory Press. 2017; p. 118323. doi:10.1101/gr.218727.116.Freely.

[49] Iin J, Fan Y, Lin X. Transformation of *Cryptococcus neoformans* by electroporation using a transient CRISPR-Cas9 expression (TRACE) system. Fungal Genetics and Biology. 2020;138:103364. doi:10.1016/j.fgb.2020.103364.

[50] Huang MY, Joshi MB, Boucher MJ, Lee S, Loza LC, Gaylord EA, et al. Short homology-directed repair using optimized Cas9 in the pathogen *Cryptococcus neoformans* enables rapid gene deletion and tagging. Genetics. 2022;220. doi:10.1093/genetics/iyab180.

[51] Lee D, Jang EH, Lee M, Kim SW, Lee Y, Lee KT, et al. Unraveling melanin biosynthesis and signaling networks in *Cryptococcus neformans*. mBio. 2019;10. doi:10.1128/mBio.02267-19.

[52] Yu CH, Chen Y, Desjardins CA, Tenor JL, Toffaletti DL, Giamberardino C, et al. Landscape of gene expression variation of natural isolates of *Cryptococcus neoformans* in response to biologically relevant stresses. Microbial Genomics. 2020;6. doi:10.1099/mgen.0.000319.

[53] Farrer RA, Voelz K, Henk DA, Johnston SA, Fisher MC, May RC, et al. Microevolutionary traits and comparative population genomics of the emerging pathogenic fungus *Cryptococcus gattii*. Philosophical Transactions of the Royal Society B: Biological Sciences. 2016;371. doi:10.1098/rstb.2016.0021.

[54] Fan W, Kraus PR, Boily MJ, Heitman J. *Cryptococcus neoformans* gene expression during murine macrophage infection. Eukaryotic Cell. 2005;4:1420–1433. doi:10.1128/EC.4.8.1420-1433.2005.

[55] Nosanchuk JD, Valadon P, Feldmesser M, Casadevall A. Melanization of *Cryptococcus neoformans* in murine infection. Molecular and Cellular Biology. 1999;19:745–750. doi:10.1128/mcb.19.1.745.

[56] Doering TL, Nosanchuk JD, Roberts WK, Casadevall A. Melanin as a potential cryptococcal defence against microbicidal proteins. Medical Mycology. 1999;37:175–181. doi:10.1046/j.1365-280X.1999.00218.x.

[57] Chai HH, Ho WK, Graham N, May S, Massawe F, Mayes S. A cross-species gene expression marker-based genetic map and QTL analysis in bambara groundnut. Genes. 2017;8. doi:10.3390/genes8020084.

[58] Tejero ME, Voruganti VS, Proffitt JM, Curran JE, Göring HHH, Johnson MP, et al. Cross-species replication of a resistin mRNA QTL, but not QTLs for circulating levels of resistin, in human and baboon. Heredity. 2008;101:60–66. doi:10.1038/hdy.2008.28.

[59] Yoshihara T, Miller ND, Rabanal FA, Myles H, Kwak IY, Broman KW, et al. Leveraging orthology within maize and *Arabidopsis* QTL to identify genes affecting natural variation in gravitropism. Proceedings of the National Academy of Sciences. 2022;119. doi:10.1073/pnas.2212199119.

[60] Bhatia A, Yadav A, Zhu C, Gagneur J, Radhakrishnan A, Steinmetz LM, et al. Yeast Growth Plasticity Is Regulated by Environment-Specific Multi-QTL Interactions. G3 Genes|Genomes|Genetics. 2014;4(5):769–777. doi:10.1534/g3.113.009142.

[61] Ba ANN, Lawrence KR, Rego-Costa A, Gopalakrishnan S, Temko D, Michor F, et al. Barcoded Bulk QTL mapping reveals highly polygenic and epistatic architecture of complex traits in yeast. eLife. 2022;11. doi:10.7554/ELIFE.73983.

[62] Sun S, Roth C, Averette AF, Magwene PM, Heitman J. Epistatic genetic interactions govern morphogenesis during sexual reproduction and infection in a global human fungal pathogen. Proceedings of the National Academy of Sciences. 2022;119:1–12. doi:10.1073/pnas.2122293119.

[63] Fu MS, Liporagi-Lopes LC, dos Santos Júnior SR, Tenor JL, Perfect JR, Cuomo CA, et al. Amoeba predation of *Cryptococcus neoformans* results in pleiotropic changes to traits associated with virulence. mBio. 2021;12. doi:10.1128/mBio.00567-21.

[64] Zhu X, Williamson PR. Role of laccase in the biology and virulence of *Cryptococcus neoformans*. FEMS Yeast Research. 2004;5:1–10. doi:10.1016/j.femsyr.2004.04.004.

[65] Lee D, Jang EH, Lee M, Kim SW, Lee Y, Lee KT, et al. Unraveling melanin biosynthesis and signaling networks in *Cryptococcus neformans*. mBio. 2019;10. doi:10.1128/mBio.02267-19.

[66] Sun S, Priest SJ, Heitman J. *Cryptococcus neoformans* mating and genetic crosses. Current Protocols in Microbiology. 2019;53:1–16. doi:10.1002/cpmc.75.

[67] Roth C, Sun S, Billmyre RB, Heitman J, Magwene PM. A high-resolution map of meiotic recombination in *Cryptococcus deneoformans* demonstrates decreased recombination in unisexual reproduction. Genetics. 2018;209:567–578. doi:10.1534/genetics.118.300996.

[68] Visscher PM, Thompson R, Haley CS. Confidence intervals in QTL mapping by bootstrapping. Genetics. 1996;143:1013–1020. doi:10.1093/genetics/143.2.1013.

[69] Churchill GA, Doerge RW. Empirical threshold values for quantitative trait mapping. Genetics. 1994;138:963–971. doi:10.1093/genetics/138.3.963.